Photochemical & Photobiological Sciences

Accepted Manuscript

This is an *Accepted Manuscript*, which has been through the Royal Society of Chemistry peer review process and has been accepted for publication.

Accepted Manuscripts are published online shortly after acceptance, before technical editing, formatting and proof reading. Using this free service, authors can make their results available to the community, in citable form, before we publish the edited article. We will replace this *Accepted Manuscript* with the edited and formatted *Advance Article* as soon as it is available.

You can find more information about *Accepted Manuscripts* in the Information for Authors.

Please note that technical editing may introduce minor changes to the text and/or graphics, which may alter content. The journal's standard Terms & Conditions and the Ethical guidelines still apply. In no event shall the Royal Society of Chemistry be held responsible for any errors or omissions in this *Accepted Manuscript* or any consequences arising from the use of any information it contains.

ROYAL SOCIETY OF CHEMISTRY

www.rsc.org/pps

Chemically reduced graphene oxide–P25–Au nanocomposite materials and their photoelectrocatalytic and photocatalytic applications

Raju Praveen and Ramasamy Ramaraj*

Department of Physical Chemistry, School of Chemistry,

Centre for Photoelectrochemistry, Madurai Kamaraj University,

Madurai - 625 021, India

*ramarajr@yahoo.com

Abstract

Visible light active photocatalysts consisting of gold nanoparticles (Au NPs) decorated chemically reduced graphene oxide–P25 nanocomposite materials (CRGO–P25–Au NCMs) were prepared through a one–pot chemical reduction method. The nanocomposite materials were characterized using diffused reflectance spectroscopy (DRS), X-ray diffraction (XRD), high-resolution transmission electron microscopy (HRTEM) and electrochemical impedance spectroscopy (EIS) analyses. The performances of the CRGO–P25–Au NCMs modified ITO electrodes were evaluated towards the photoelectrochemical oxidation of methanol. The photoelectrode fabricated using CRGO–P25–Au NCM exhibited a higher photocurrent of 293μA/cm^2 compared to the other controlled electrodes. The CRGO–P25–Au NCMs were also used for the photocatalytic reduction of highly toxic chromium(VI) ions to chromium(III) ions in the presence of oxalic acid as a sacrificial electron donor. The results showed that around 75% of the Cr(VI) ions were photocatalytically reduced to Cr(III) ions by the CRGO–P25–Au NCM within the light irradiation time of 1 h. In both the applications, the enhanced catalytic activity of the CRGO–P25–Au NCM was attributed to the improved visible light absorption and reduced charge recombination exerted by the interaction of CRGO and Au NPs with P25 and their synergistic effect.

Keywords: Chemically reduced graphene oxide, P25, Gold nanoparticles, Photoelectrochemical oxidation, Photocatalytic reduction

Photochemical & Photobiological Sciences Accepted Manuscript

Introduction

Solar energy is regarded as a sustainable alternative to the rapidly depleting fossil fuels and only a meagre portion of that valuable energy is converted into useful forms of energy [1]. Utilization of solar energy is the best way to produce different forms of energy and to develop environment remediation technologies. Photon energy assisted hydrogen production, methanol oxidation, organic dye degradation and inorganic toxic metal ions (chromium (VI) and mercury (II)) reduction are the most promising among them and moreover they are well recognized.

Titanium dioxide (TiO_2) is one of the most important semiconductor materials used in the fields of photoelectrochemistry and photocatalysis, because of its redox behaviour, stable against chemical corrosion and photocorrosion, low-cost and non-toxic [2–4]. The charge recombination is the most crucial function which affects the photocatalytic efficiency of TiO_2. Therefore, it is important to develop photocatalysts with improved interfacial charge transfer property and high photocatalytic efficiency. Graphene is a well-known two-dimensional carbon material which has been used for numerous energy and environmental remediation applications, because of its high electron conductivity, thermal stability and low-cost. [5–6]. Recently, researchers have reported that the reduced graphene oxide/semiconductor nanocomposite materials (for example CRGO/TiO_2 or ZnO NCMs) exhibited interesting photocatalytic properties when compared to their pristine semiconductors. Zhang *et al.* reported that the hydrothermally synthesised chemically bonded P25–GR composites exhibited enhanced photocatalytic degradation of methylene blue [7]. Lightcap *et al.* demonstrated that the photogenerated electrons were partially stored in the RGO mat because of its electron conducting nature [8]. The Au/TiO_2 NCMs showed better photocatalytic reduction of toxic Cr(VI) ions [9] and photoelectrocatalytic oxidation of methanol [10]. The Au NPs act as electron sink for photoinduced electrons which prevent rapid charge recombination and thereby, facilitate the interfacial charge transfer process in the photocatalytic systems.

Precious metals are used in direct methanol fuel cells (DMFCs) as both anode and cathode and however, the CO adsorption and temperature are found to be the drawbacks of DMFCs [11-12]. In the photoelectrochemical methanol oxidation we can alter the anode materials with low-cost semiconductor materials and tune the photocurrent production efficiency [13-14]. The Cr(VI) compounds have found numerous applications viz., electroplating, leather tanning and metal finishing and as a

Photochemical & Photobiological Sciences Accepted Manuscript

consequence, large quantities of aqueous Cr(VI) wastes are discharged into the environment in the absence of proper pretreatment. Furthermore, trace amounts of Cr(VI) in drinking water causes bladder and skin cancer and affects liver and kidney [9,15–16]. Herein, we report the preparation of CRGO–P25–Au NCMs through a one–pot chemical reduction method to evaluate their performances towards energy and environmental remediation applications. The nanocomposite photocatalysts were effectively utilized for the photoelectrocatalytic oxidation of methanol and photocatalytic reduction of Cr(VI) to Cr(III) ions. The bi-functional visible light active nanocomposite photocatalysts would be an affordable material for energy and environmental remediation applications.

Experimental section

Materials

Graphite was purchased from Alfa Aesar. TiO_2 (P25) was purchased from Acros organics. Hydrogen tetrachloroaurate trihydrate ($HAuCl_4.3H_2O$) was received from Sigma-Aldrich. All other chemicals used in this investigation were obtained from Merck and used as received without further purification. Indium doped tin oxide (ITO) coated conducting glass plate with a surface resistance of 4-8 Ω sq^{-1} (CG-411N-1507) (Delta Technologies Ltd., USA) was used to prepare modified electrodes. All glassware was thoroughly cleaned with aqua regia and rinsed extensively with doubly distilled water before use.

Characterization

Absorption spectra were recorded using an Agilent 8453 spectrophotometer. Diffused reflectance spectra (DRS) were recorded using a JASCO V-650 double beam UV–visible spectrophotometer, equipped with ISV–722/60 mm sphere diffuse reflectance accessories. X-ray diffraction (XRD) patterns of the NCMs were obtained with a XPERT-PRO-PANalytical instrument with Cu Kα radiation (λ = 1.5406 Å). High resolution transmission electron microscopy (HRTEM) analysis were conducted using a JEOL JEM 2100 instrument operated at 200 kV.

Preparation of CRGO–P25–Au NCMs

Graphene oxide (GO) was prepared by a modified Hummer's method [17]. GO solution was prepared by sonicating the graphite oxide powder (2 mg) dispersed in 20 mL of double distilled water for 2 h. For the preparation of CRGO–P25–Au NCMs, Au NPs were deposited on the CRGO–P25 nanocomposite through a simple one–pot

Photochemical & Photobiological Sciences Accepted Manuscript

chemical reduction method. In the preparation, 200 mg of P25 (TiO_2) nanoparticles were added into the GO solution and sonicated for 15 min, followed by 30 min of stirring. To this mixture, a freshly prepared $NaBH_4$ solution (5%) was added to achieve the reduction of GO. Finally, aqueous $HAuCl_4$ (0.5, 1, 2, 3 and 5 mM) solution was added to a 20 ml of CRGO–P25 solution. After a vigorous stirring of 3 h, a freshly prepared $NaBH_4$ solution (5%) was added to reduce Au(III) to Au NPs. The obtained NCMs were labelled as CRGO–P25–Au(0.5), CRGO–P25–Au(1), CRGO–P25–Au(2), CRGO–P25–Au(3) and CRGO–P25–Au(5), respectively. After the 5 h of stirring, the final products were subjected to several washings using double distilled water and ethanol. The washed samples were centrifuged and the solid samples were dried in a hot air oven at 80 °C. Similarly, the controlled samples CRGO–P25 and P25–Au NPs were prepared in the absence of $HAuCl_4$ and GO, respectively.

Photoelectrochemical studies

The photoelectrocatalytic experiments were performed using a CH Instruments Electrochemical Workstation (Model-760D). The photoelectrochemical experiments were conducted using a single compartment three electrode cell. The modified ITO photoelectrode (1 cm^2) was used as a working electrode and platinum wire was employed as a counter electrode. The reference electrode was silver/silver chloride (Ag/AgCl) electrode. The supporting electrolyte was 0.1 M Na_2SO_4 and the solution was deaerated by purging nitrogen gas in dark before starting each experiment. A 450 W Xenon lamp was used as a light source with water filter cell 6 cm path length with pyrex glass windows to cut off the far UV and IR radiation. The modified ITO photoelectrodes were fabricated using 5 mg of the CRGO–P25–Au NCMs, CRGO–P25, P25–Au NPs and P25, dispersed in 1 ml of 2–propanol and sonicated for 10 min to ensure the homogeneous dispersion. The nanocomposite solutions were drop-casted on the ITO electrodes and dried under dark. The same modified ITO photoelectrodes were used for electrochemical impedance spectra (EIS) analysis. A 1 mM of $K_3Fe(CN)_6$ in 0.1 M PBS and 0.1 M KCl was used as a redox analyte. The modified photoelectrodes and their corresponding open circuit potential were employed as the electrode potential with a frequency range of 1-100 KHz.

Photocatalytic studies

The photocatalytic study was carried out in a glass cell system at room temperature [9]. The CRGO–P25–Au NCMs, CRGO–P25, P25–Au and P25 (10 mg) were separately dispersed in the photolysis cell containing 20 ml of 0.4 mM $K_2Cr_2O_7$

Photochemical & Photobiological Sciences Accepted Manuscript

and 4 mM oxalic acid (OA) mixture and then illuminated using light source. Before the illumination, nitrogen gas was purged into the reaction mixture for 30 min under dark with constant stirring. A 250 W tungsten–halogen lamp was used as a light source. The sample aliquots were taken from the reaction solutions at a regular time intervals and were examined in spectrophotometer for Cr(VI) reduction. The Cr(VI) ions were estimated by diphenylcarbazide method at 540 nm by analyzing the complex formed upon the addition of colorimetric reagent 1,5-diphenylcarbazide [9,18].

Results and discussion

Absorption and band–gap studies

The diffused reflectance spectra (DRS) of the CRGO–P25–Au NCMs and CRGO–P25 were recorded and shown in Figure 1A. The observation of surface plasmon resonance (SPR) band at around 550 nm (Fig.1A) confirmed the formation of Au NPs in the CRGO–P25–Au NCMs through the one–pot chemical reduction method. The P25 did not show the visible light absorption. However, after the incorporation of GO with P25, the visible light absorption region was extended and as a consequence, the CRGO–P25 band-gap edge was shifted towards lower energy side. The P25 nanoparticles were anchored on the GO matrix and the GO reduction was occurred [7]. Sodium borohydride was used as a reducing agent for the reduction and deposition of Au NPs on the CRGO–P25 surface [10,19]. The absorbance of the CRGO–P25–Au NCMs increased with respect to the increase in the concentration of Au NPs (0.5, 1, 2 and 3 mM of gold precursor). The band–gap (E_{bg}) values of the NCMs were calculated using *Tauc`s* plot method (Figure S1). The E_{bg} values were obtained by extrapolating the linear region of the plot of $(\alpha h\nu)^{1/2}$ *vs*. $h\nu$. The E_{bg} of P25 (3.2 eV) decreased to 2.85, 2.75, 2.72, 2.69 and 2.66 eV for CRGO–P25, CRGO–P25–Au(0.5), CRGO–P25–Au(1), CRGO–P25–Au(2) and CRGO–P25–Au(3), respectively. The calculated E_{bg} values of the different NCMs with different amounts of Au NPs and their corresponding absorption wavelengths are shown in Figure 1B, which indicates that the E_{bg} values of P25 were decreased after the incorporation of CRGO and Au NPs. The extension of absorption could be attributed to the chemical interaction between the P25 and GO in the CRGO–P25 NCM [7]. The intensity of the SPR band of Au NPs increased with increasing amounts of Au NPs [20] in the CRGO–P25–Au NCMs and the absorption of P25 was also extended to the visible light region. This enhanced visible light absorption could improve the photocatalytic

Photochemical & Photobiological Sciences Accepted Manuscript

activity of P25. Figure 1B clearly indicated the red shift in the band-gap of P25 and enhanced visible light absorption.

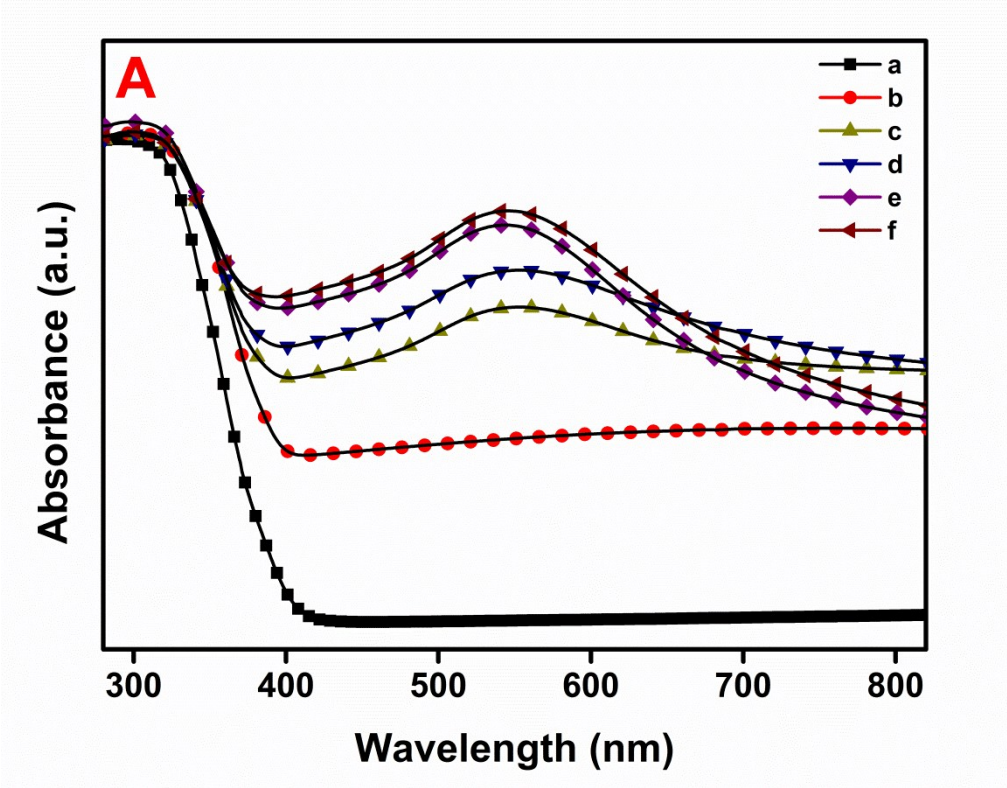

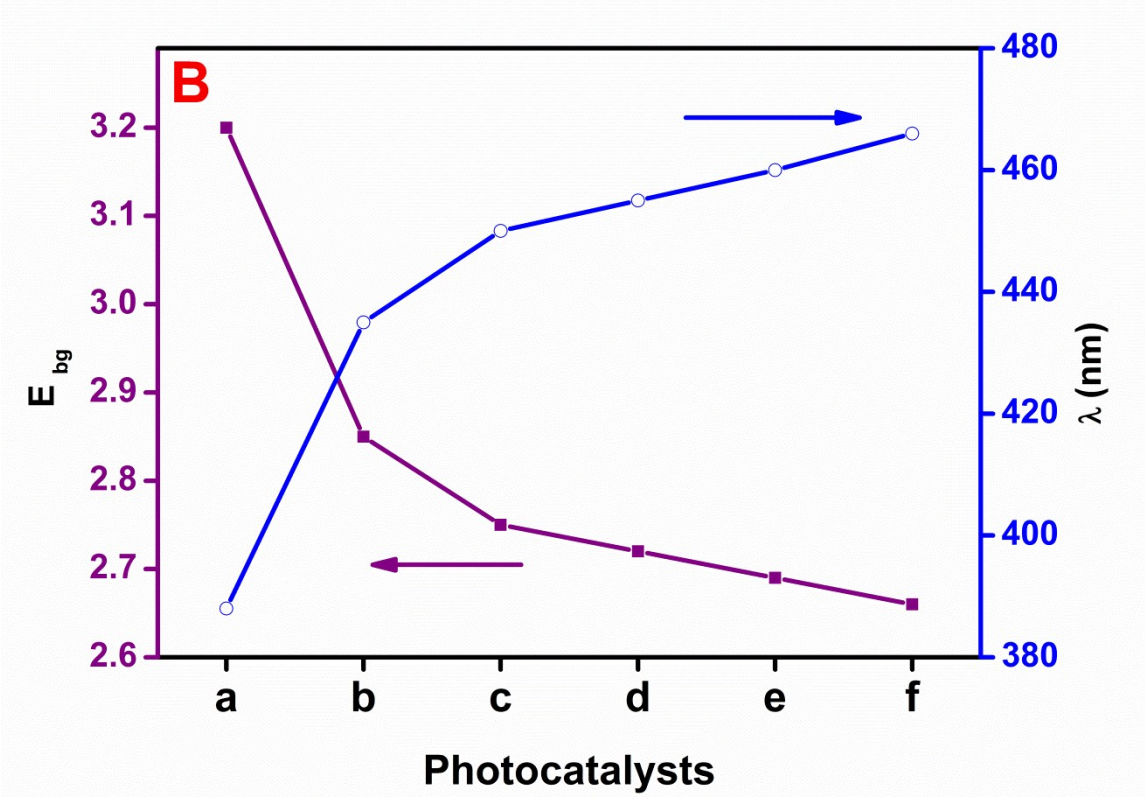

Photochemical & Photobiological Sciences Accepted Manuscript

Figure 1. Diffused reflectance spectra (A) and band–gap energy (E_{bg}) (B) with the corresponding absorption wavelength of P25 (a), CRGO–P25 (b), CRGO–P25–Au(0.5) (c), CRGO–P25–Au(1) (d), CRGO–P25–Au(2) (e) and CRGO–P25–Au(3) (f) NCMs.

XRD and HRTEM analyses

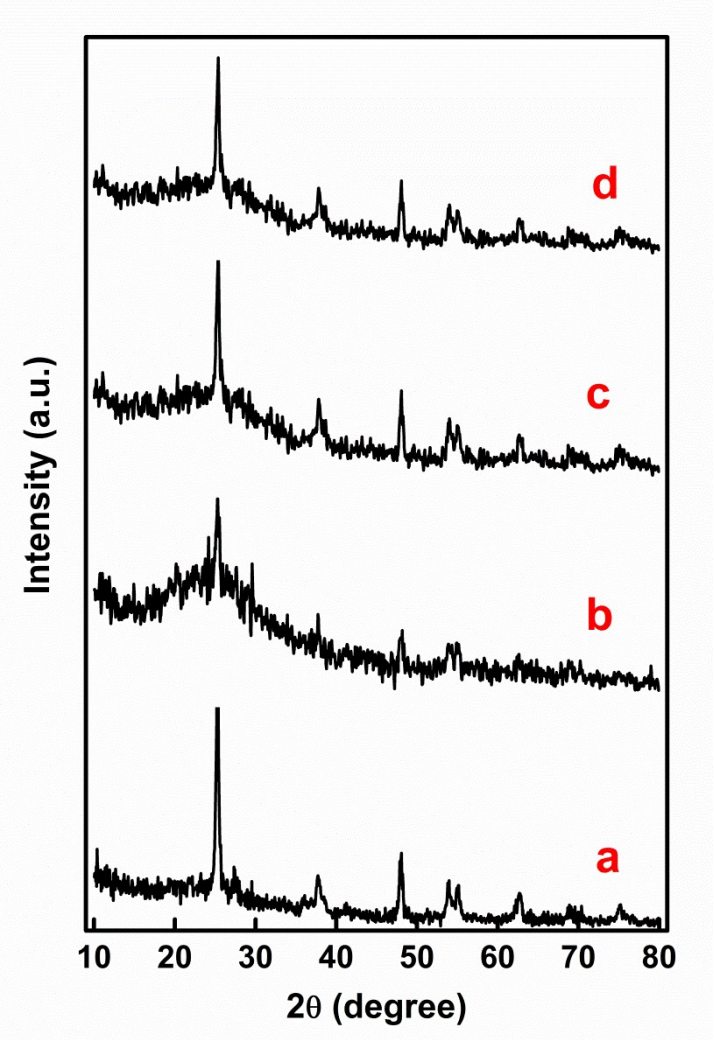

Figure 2. XRD patterns of P25 (a), CRGO–P25 (b), CRGO–P25–Au(1) (c) and CRGO–P25–Au(3) (d) NCMs.

XRD patterns were recorded for the Au NPs deposited CRGO–P25–Au, CRGO–P25 and P25 nanomaterials (Figure 2). The anatase phase of P25 was clearly confirmed through the XRD pattern (Figure 2(a)) and the diffraction peaks observed at the 2θ values of 25.2, 37.8, 48.2, 53.9 and 55.3° were corresponding to the diffraction planes of (1 0 1), (0 0 4), (2 0 0), (1 0 5) and (2 1 1), respectively. The rutile phase of P25 with a diffraction peak value of 62.6° was observed for the diffraction plane of (3 1 0) [JCPDS Card No. 86-1156]. After the incorporation of

Photochemical & Photobiological Sciences Accepted Manuscript

GO with P25, no characteristic diffraction peak corresponding to GO was observed in the XRD pattern (Figure 2(b)), because of the presence of very low content of GO in CRGO–P25 nanocomposite. The Au diffraction peaks observed at 39.2, 44.4 and 64.4° correspond to the diffraction planes of (1 1 1), (2 0 0) and (2 2 0), respectively (Figure 2(c and d)) [JCPDS Card No. 4-0784]. The anatase crystalline nature of P25 was not altered after the incorporation of CRGO and Au, because of their very low amounts in the nanocomposites. Figure 3 shows the HRTEM images of the CRGO–P25 and Au NPs deposited CRGO–P25–Au(3) NCM. These images clearly indicated that the P25 nanoparticles were deposited on the CRGO surface (Figure 3A). Figure 3B shows that the Au NPs with a size of <10 nm were deposited on the P25 nanoparticles surface in the CRGO–P25 composite. The presence of CRGO and Au NPs were expected to improve the photogenerated charge separation in order to achieve the efficient photocatalytic applications.

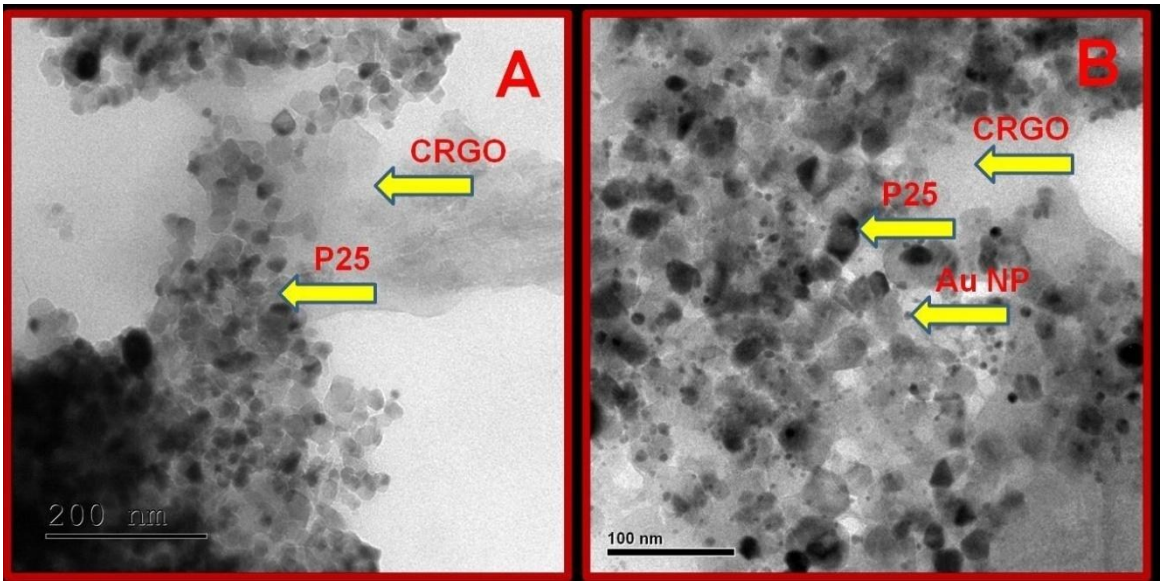

Figure 3. HRTEM images of CRGO–P25 (A) and Au NPs deposited CRGO–P25–Au(3) (B) NCMs.

Photoelectrochemical oxidation of methanol

The photoelectrochemical responses of the CRGO–P25–Au NCMs modified photoelectrodes were investigated by immersing the electrodes in a photoelectrochemical cell containing a mixture of 0.1 M CH_3OH and 0.1 M Na_2SO_4 under light "on-off" conditions (Figure 4A). The linear sweep voltammograms (LSVs) were recorded in the potential range between –0.5 V and 1 V for the P25, CRGO–

Photochemical & Photobiological Sciences Accepted Manuscript

P25 and CRGO–P25–Au NCMs modified photoelectrodes in the presence of 0.1 M CH_3OH and are shown in Figure 4. Figure 4A displays the comparisons of LSVs recorded for different modified photoelectrodes under light "on-off" conditions. The CRGO–P25–Au(1) modified photoelectrode produced a higher photocurrent under light illumination condition. The anodic scan of LSV clearly indicated that the photocurrent was increased while increasing the applied potential under light illumination condition. The steady state photocurrent was attained from –0.2 V in the given potential window. Under light "on-off" conditions, a fast increase and decrease responses in the photocurrent were observed because of the photocurrent generation under light "on-off" conditions. The CRGO–P25–Au(1) modified photoelectrode exhibited a 4.7 and 2 fold higher photocurrent compared to the P25 and CRGO–P25 modified photoelectrodes, respectively. Figure S2 shows the comparisons of the LSV responses of P25, CRGO–P25, CRGO–P25–Au(0.5), CRGO–P25–Au(1), CRGO–P25–Au(2) and CRGO–P25–Au(3) modified photoelectrodes under dark and light irradiation conditions. The modified photoelectrodes did not show any photocurrent response under dark condition and however, the photocurrent was observed only under light irradiation condition. This observation revealed that the photoinduced charge separation and electron transfer occurred effectively at the CRGO–P25–Au NCM modified photoelectrodes. The best photoelectrocatalytic methanol oxidation performance was observed due to the synergetic effect of CRGO and Au NPs present on the P25. The CRGO acted as an effective electron acceptor and conduction matrix for the photoinduced electrons at the P25 coated electrode. The photogenerated electrons were not subjected to charge recombination at the P25 due to the presences of the Au NPs which acted as an electron sink [21–22]. Further, the adsorbed methanol molecules at the CRGO–P25-Au NCM were effectively oxidized by photogenerated holes and as a consequence, higher photocurrent was produced. Because of the presence of Au NPs in the NCMs, Schottky barrier junction was formed at the Au NPs and P25 interface and enhanced the interfacial charge transfer process. In the absence of CRGO and Au NPs, the P25 and CRGO–P25 modified photoelectrodes showed poor photoelectrocatalytic oxidation of CH_3OH compared to the CRGO–P25–Au(1) modified photoelectrode (Figure 4). The Au NPs acted as a sink for the excited electrons and enhanced the photoinduced charge separation process.

Photochemical & Photobiological Sciences Accepted Manuscript

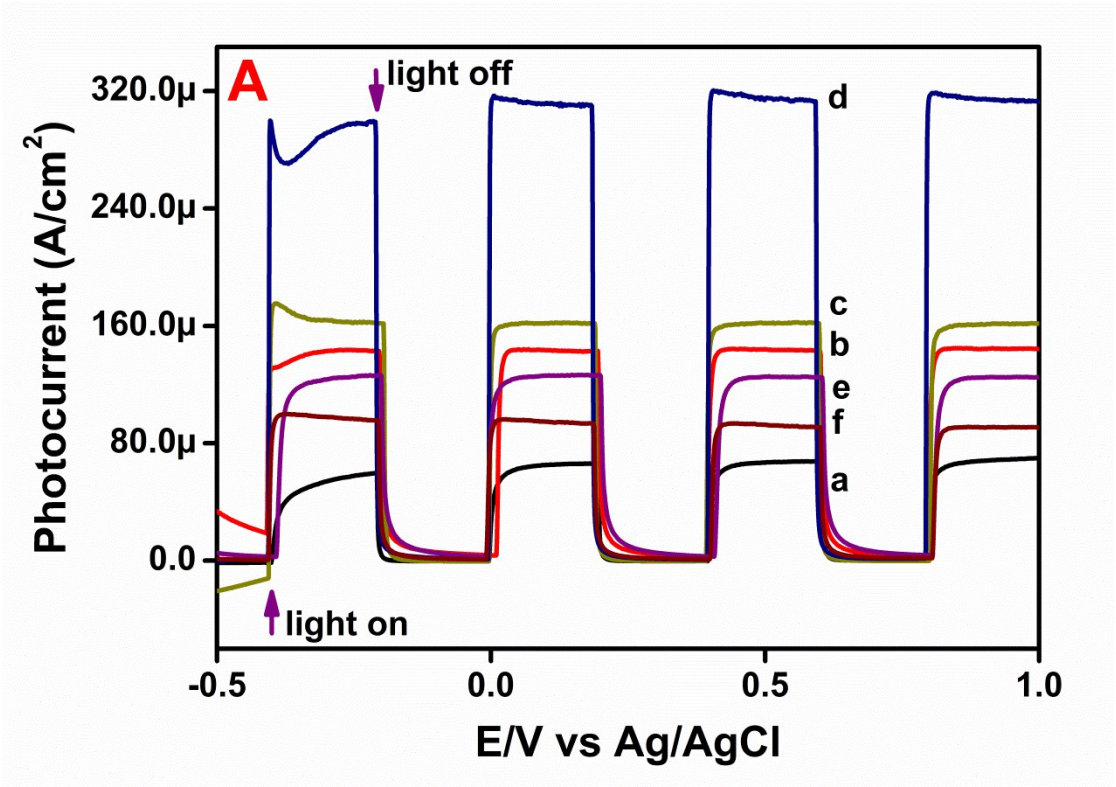

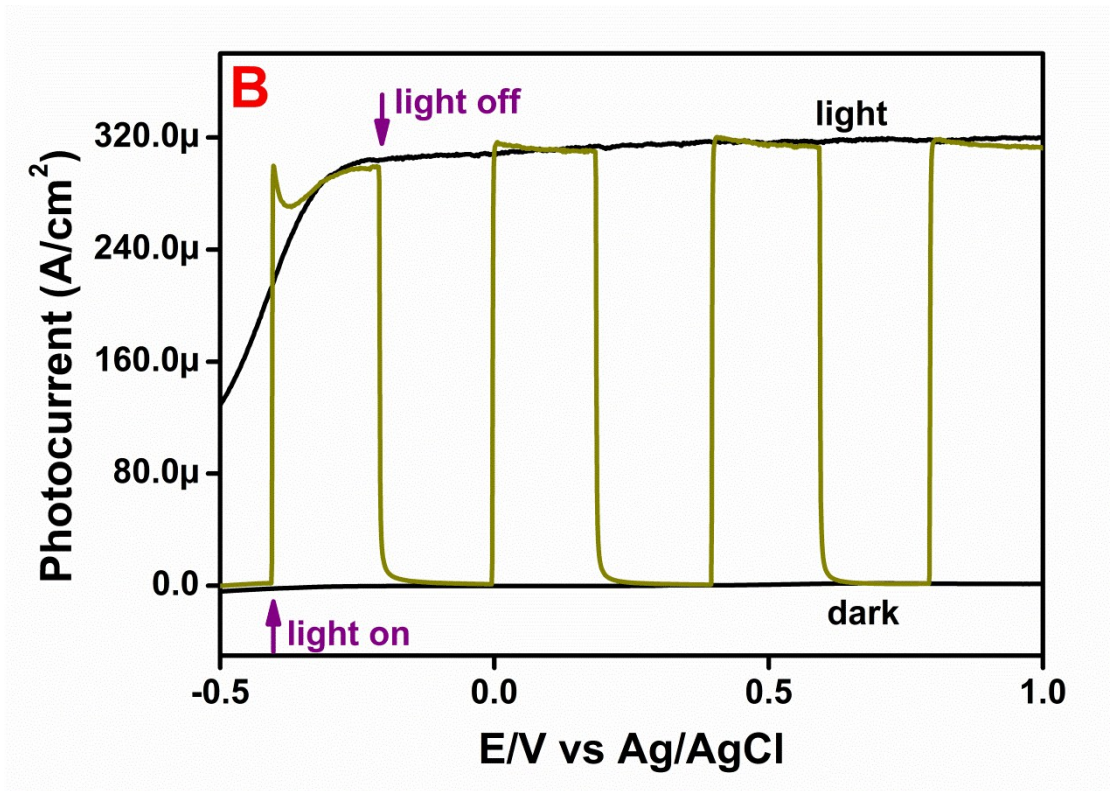

Figure 4. Comparison of LSV curves obtained for P25 (a), CRGO–P25 (b), CRGO–P25–Au(0.5) (c), CRGO–P25–Au(1) (d), CRGO–P25–Au(2) (e) and CRGO–P25–Au(3) (f) modified photoelectrodes under light "on-off" conditions (A). LSV curves obtained for the CRGO–P25–Au(1) NCM modified photoelectrode under "dark", "light" and

Photochemical & Photobiological Sciences Accepted Manuscript

"light on-off" conditions. The photoelectrochemical cell solution contained a mixture of 0.1 M CH_3OH in 0.1 M Na_2SO_4 (B).

The photocurrent measurement was carried out at an applied potential +0.6 V for the modified photoelectrodes under light "on-off" conditions, towards the photoelectrocatalytic oxidization of CH_3OH. Figure 5A shows the comparison of anodic photocurrents observed for the P25, CRGO–P25, CRGO–P25–Au(0.5), CRGO–P25–Au(1), CRGO–P25–Au(2) and CRGO–P25–Au(3) modified photoelectrodes in the presence of the solution containing 0.1 M each Na_2SO_4 and CH_3OH. The increase and decrease in the photocurrents were reproducible during the light "on-off" cycles. The photocurrent generation showed two steps: first step was the rapid response of photocurrent against the light illumination and the second step was the attainment of steady state photocurrent. The CRGO–P25–Au(1) modified photoelectrode showed a higher photocurrent of 293 $\mu A/cm^2$. The obtained photocurrents were 63, 135, 162, 293, 120 and 85 $\mu A/cm^2$ for the modified photoelectrodes P25, CRGO–P25, CRGO–P25–Au(0.5), CRGO–P25–Au(1), CRGO–P25–Au(2) and CRGO–P25–Au(3), respectively. Based on these results, the CRGO–P25–Au(1) modified photoelectrode was chosen to measure the CH_3OH concentration dependent photocurrent. The steady state photocurrent was progressively increased while increasing the CH_3OH concentration and reached a maximum. Figure 5B shows the plot of CH_3OH concentration *vs.* photocurrent for the CRGO–P25–Au(1) NCM modified photoelectrode. As shown in the inset of Figure 5B, the steady state photocurrent was directly proportional at the lower concentration of CH_3OH. It clearly indicated that the photoelectrochemical oxidation rate of CH_3OH at the CRGO–P25–Au(1) modified photoelectrode followed a first order kinetics with respect to the CH_3OH concentration. At the increasing CH_3OH concentration, the photocurrent reached a maximum level due to the high concentration of CH_3OH molecules with insufficient photogenerated holes at the CRGO–P25–Au(1) modified photoelectrode. The CRGO–P25–Au(1) modified photoelectrode generated a constant photogenerated holes for every invariable light irradiation at the same applied potential.

Photochemical & Photobiological Sciences Accepted Manuscript

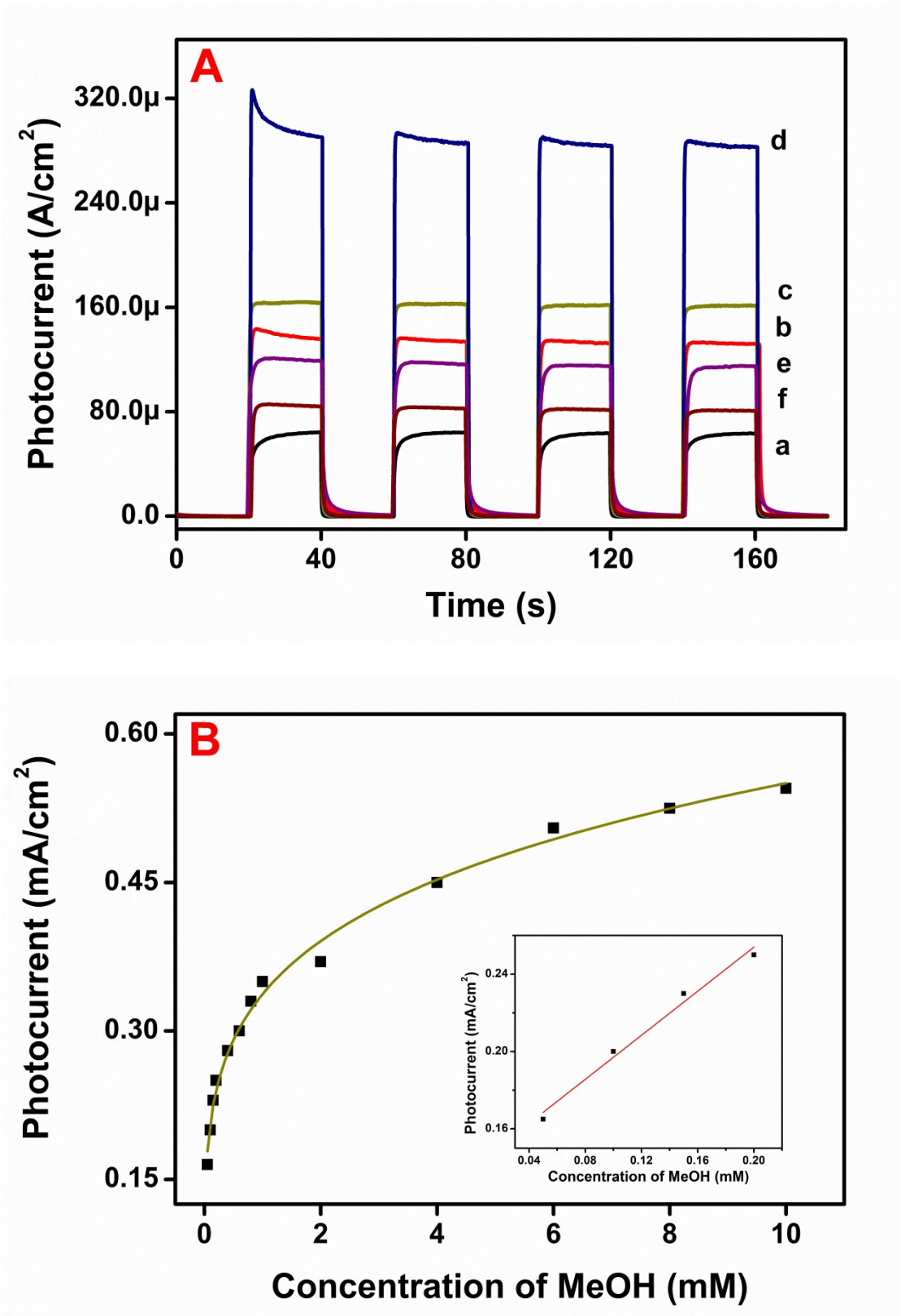

Figure 5. Photocurrent–time characteristics recorded at the applied potential of +0.6 V for P25 (a), CRGO–P25 (b), CRGO–P25–Au(0.5) (c), CRGO–P25–Au(1) (d), CRGO–P25–Au(2) (e) and CRGO–P25–Au(3) (f) modified photoelectrodes under light "on-

Photochemical & Photobiological Sciences Accepted Manuscript

off" conditions. The photoelectrochemical cell solution was a mixture of 0.1 M CH_3OH in 0.1 M Na_2SO_4 (A). Dependence of photocurrent against methanol concentration at the CRGO–P25–Au(1) modified photoelectrode at an applied potential of +0.6 V under light "on-off" conditions (B).

Electrochemical impedance analysis

Electrochemical impedance spectroscopy (EIS) is a very useful technique to analyse the electrical properties of the modified photoelectrodes in an electrochemical cell. The EIS of the selected modified photoelectrodes of P25, CRGO–P25 and CRGO–P25–Au(1) at their corresponding open circuit potential were recorded under dark and light illumination conditions [23]. Figure 6 shows the Nyquist plots of CRGO–P25–Au(1) modified photoelectrode under dark and light illumination conditions and Figure S3 shows the Nyquist plots of P25, CRGO–P25 modified photoelectrodes under dark and light illumination conditions. The obtained Nyquist plots were fitted to Randles equivalent circuit model [$R_s(C_{dl}(R_{ct}Z_W))$] (Figure 6(inset)) using ZSimpWin software. In this model, the solution resistance (R_s) and double layer capacitance (C_{dl}) were connected in series circuit and the charge transfer resistance (R_{ct}) and Warburg impedance (Z_W) are connected with C_{dl} in a parallel circuit. The Nyquist plot obtained from the EIS showed a semicircle at higher frequencies corresponding to the electron-transfer-limited process and the linear portion at lower frequencies corresponding to the diffusion-limited process. The obtained electron-transfer resistance (R_{ct}) values of P25, CRGO–P25 and CRGO–P25–Au(1) modified photoelectrodes under "dark" and "light" illumination conditions are provided in Table 1. The results from EIS Nyquist plots disclosed that the R_{ct} values of the CRGO–P25–Au(1) modified photoelectrode were lower than those of the P25 and CRGO–P25 modified photoelectrodes under both "dark" or "light" illumination conditions. The higher photocurrent produced under "light" illumination condition could be attributed to the lower R_{ct} value of the CRGO–P25–Au(1) modified photoelectrode with improved electron conducting behaviour. Thus, in the presence of CRGO and Schottky barrier interaction between Au NPs and P25, the photoinduced electron transfer process was very effective at the CRGO–P25–Au(1) modified photoelectrode.

Photochemical & Photobiological Sciences Accepted Manuscript

Table 1. Charge transfer resistance (R_{ct}) values observed for the photoelectrodes.

Modified photoelectrode	Charge transfer resistance (R_{ct}), Ω	
	Dark	Light
P25	5197	827
CRGO–P25	1597	229
CRGO–P25–Au(1)	298	146

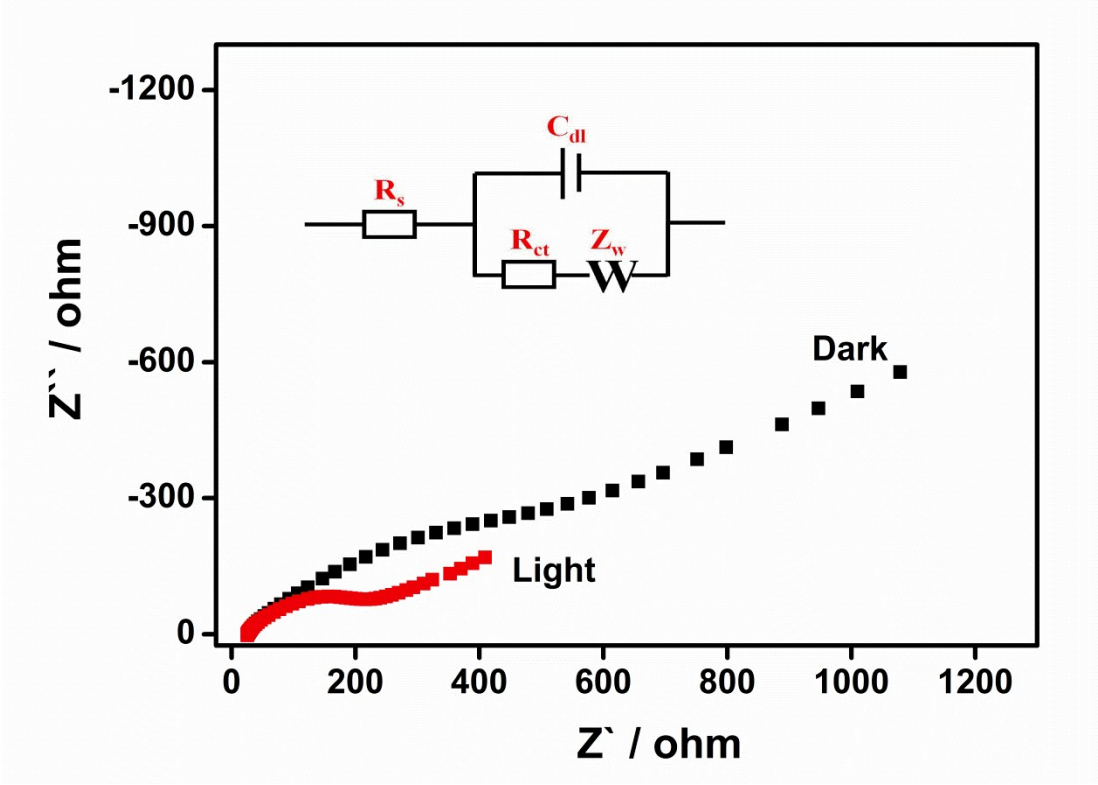

Figure 6. EIS Nyquist plots recorded for CRGO–P25–Au(1) NCM modified photoelectrode under dark and light illumination conditions. Inset: Equivalent circuit.

Photocatalytic reduction of Cr(VI) ions

The Cr(VI) ions are considered as highly toxic and carcinogenic whereas Cr(III) is one of the essential nutrients for body functioning. The Cr(VI) was chosen for the photocatalytic reduction study. The photocatalytic activity of the P25, CRGO–P25, CRGO–P25–Au(0.5), CRGO–P25–Au(1), CRGO–P25–Au(2), CRGO–P25–Au(3) and CRGO–P25–Au(5) NCMs was studied towards the reduction of Cr(VI) ions under light illumination in the presence of oxalic acid as a sacrificial electron donor, and their corresponding degradation profiles and kinetic plots are shown in Figure 7. The CRGO–P25–Au(3) NCM photocatalyst exhibited a better photocatalytic reduction

Photochemical & Photobiological Sciences Accepted Manuscript

efficiency of 75% for the reduction of Cr(VI) to Cr(III) in a light illumination of 1 h. The plot of irradiation time *vs.* ln (C_t/C_0) showed a linear relationship, which suggested that the photoreduction of Cr(VI) proceeded *via* a pseudo first order kinetics. The rate constant values (k) calculated for the P25, CRGO–P25, CRGO–P25–Au(0.5), CRGO–P25–Au(1), CRGO–P25–Au(2), CRGO–P25–Au(3) and CRGO–P25–Au(5) NCMs photocatalysts are 0.004, 0.002, 0.006, 0.009, 0.012, 0.021 and 0.080 min^{-1}, respectively. The photocatalytic reduction efficiency was gradually increased for the CRGO–P25-Au NCMs with increasing the Au content compared to the P25 and CRGO–P25, owing to the fact that the presence of CRGO and Au NPs improved the photoinduced charge separation effectively through the interfacial interaction between CRGO–P25 and Au NPs. The photocatalytic reduction efficiency was negligible in the absence of CRGO and Au NPs. Moreover, the interfacial charge transfer process was increased *via* the Fermi level equilibration between the P25 and Au NPs, and as a consequence, the Cr(VI) ions were effectively reduced by the photogenerated electrons. The presence of CRGO enhanced the electron conducting nature at the photocatalyst. The photocatalytic degradation profile of P25–Au(3) NCM photocatalyst with and without graphene oxide is shown in Figure S4 and an enhanced photocatalytic activity was observed for the CRGO–P25–Au(3) NCM photocatalyst.

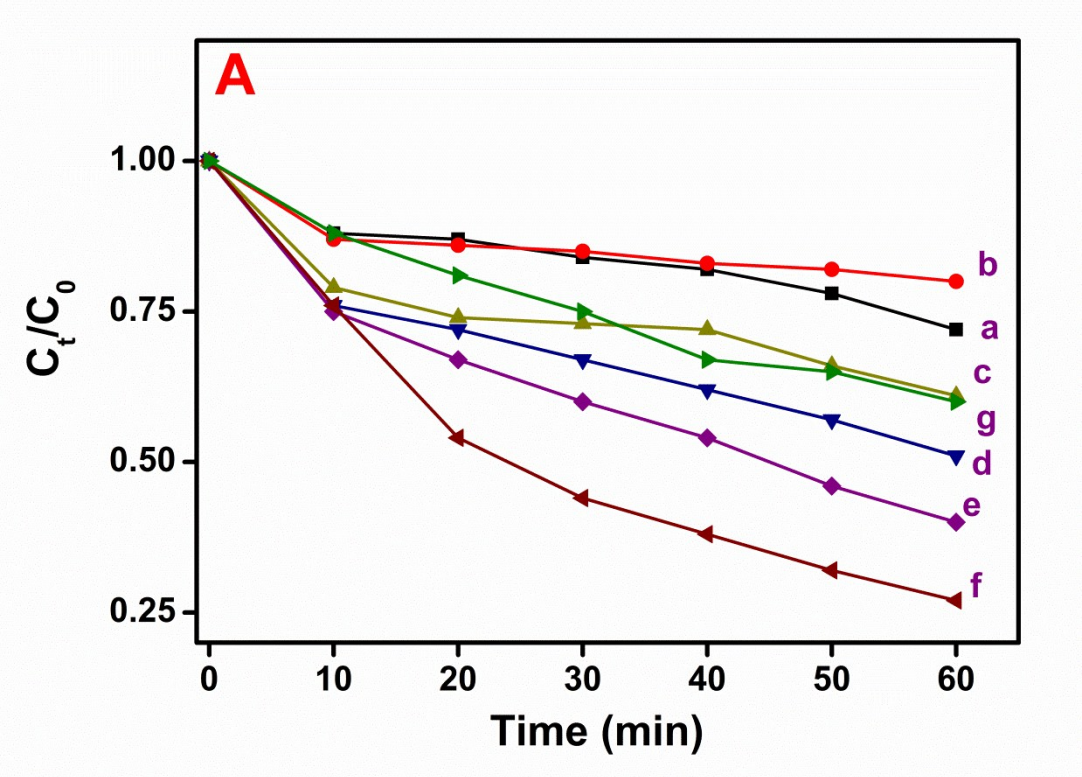

Photochemical & Photobiological Sciences Accepted Manuscript

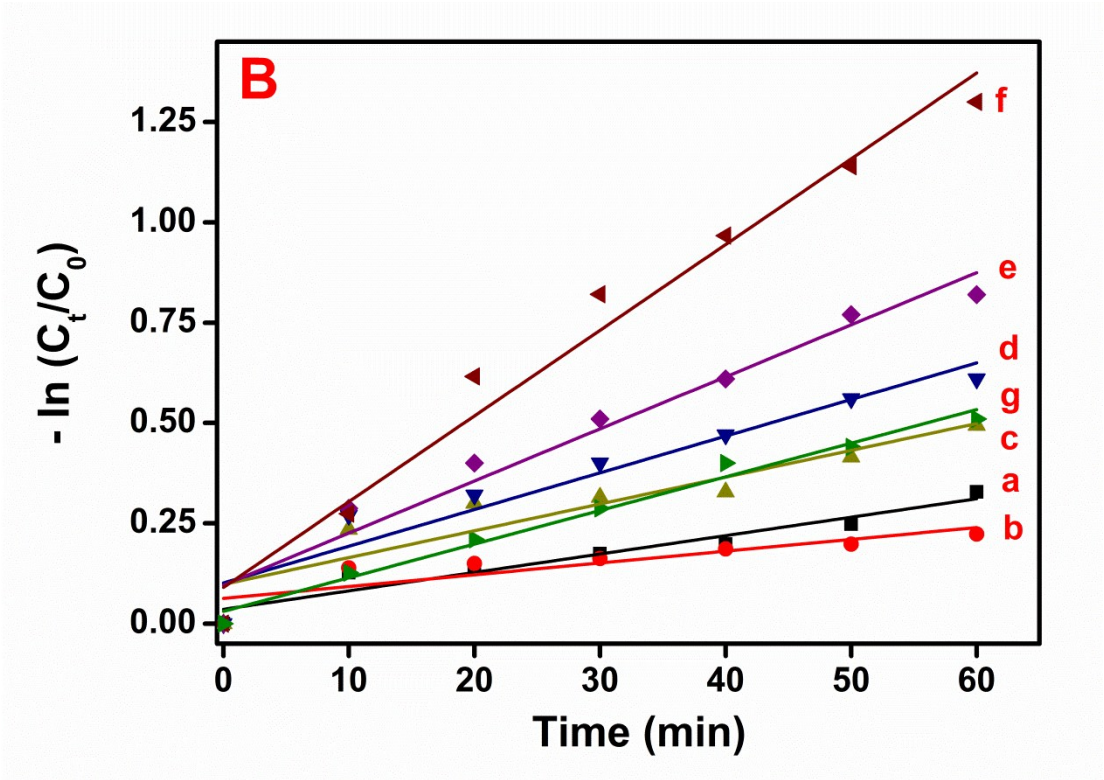

Figure 7. Photocatalytic reduction profiles (A) and corresponding kinetic plots (B) obtained for the photocatalytic reduction of Cr(VI) ions at P25 (a), CRGO–P25 (b), CRGO–P25–Au(0.5) (c), CRGO–P25–Au(1) (d), CRGO–P25–Au(2) (e) and CRGO–P25–Au(3) (f) and CRGO–P25–Au(5) (g) NCMs under light illumination in the presence of oxalic acid. Concentration of Cr(VI) ions and oxalic acid were 0.4 mM and 4 mM, respectively.

Conclusions

In conclusion, the visible light absorbing CRGO–P25–Au NCMs photocatalysts were successfully prepared through a facile one-pot chemical reduction method and characterized using DRS, XRD, HRTEM and EIS. The prepared NCMs were used for the two different applications *viz.*, the photoelectrocatalytic oxidation of methanol and photocatalytic reduction of Cr(VI) to Cr(III) ions. The CRGO–P25–Au(1) NCM modified photoelectrode showed the best photoelectrochemical performance for methanol oxidation with a highest photocurrent production of 293 μA/cm^2 than that of other controlled photoelectrodes. In the photocatalytic reduction of Cr(VI) ions to Cr(III) ions, the CRGO–P25–Au(3) NCM photocatalyst exhibited higher efficiency compared to the other NCMs. The better performance was attributed to the synergistic effect of the CRGO and Au NPs at the P25. The band-gap (E_{bg}) edge was shifted to visible region for the P25 (TiO_2) in the presence of Au NPs. The interaction of Au

Photochemical & Photobiological Sciences Accepted Manuscript

NPs with CRGO–P25 brought about the Schottky barrier junction formation which enhanced the charge separation process at the photocatalysts. This bi-functional nanocomposite photocatalyst CRGO–P25–Au could be efficiently used for solar energy conversion and environment remediation applications.

Supporting Information Available:

The *Tauc`s* plots of NCMs. The LSV responses in dark and light illumination conditions for the modified photoelectrodes. The Nyquist plots of P25 and CRGO–P25 modified photoelectrodes in dark and light illumination conditions. The comparison of photocatalytic reduction efficiency of CRGO–P25–Au(3) NCM with and without graphene oxide.

Acknowledgement

The financial support received from the Science and Engineering Research Board (SERB), Government of India, New Delhi is gratefully acknowledged. The authors thank Dr. Anuradha M. Ashok, PSG Institute of Advanced Studies, Coimbatore, for the HRTEM analysis.

References

1. K. Kalyanasundaram and M. Graetzel, Artificial photosynthesis: Biomimetic approaches to solar energy conversion and storage, *Curr. Opin. Biotechnol.* 2010, **21**, 298–310.
2. A. Fujishima and K. Honda, Electrochemical Photolysis of Water at a Semiconductor Electrode, *Nature,* 1972, **238**, 37–38.
3. K. Hashimoto, H. Irie and A. Fujishima, TiO_2 Photocatalysis: A Historical Overview and Future Prospects, *Jpn. J. Appl. Phys*., 2005, **44**, 12, 8269–8285.
4. X. Chen and S.S. Mao, Titanium Dioxide Nanomaterials: Synthesis, Properties, Modifications, and Applications, *Chem. Rev*., 2007, **107**, 2891–2959.
5. X. An and J.C. Yu, Graphene-based photocatalytic composites, *RSC Adv*., 2011, **1**, 1426–1434.
6. D. Chen, H. Feng and J. Li, Graphene Oxide: Preparation, Functionalization, and Electrochemical Applications, *Chem. Rev*., 2012, **112**, 6027–6053.
7. H. Zhang, X. Lv, Y. Li, Y. Wang and J. Li, P25-Graphene Composite as a High Performance Photocatalyst, *ACS Nano,* 2010, **4**, 380–386.
8. I. V. Lightcap, T. H. Kosel and P. V. Kamat, Anchoring Semiconductor and Metal Nanoparticles on a Two-Dimensional Catalyst Mat. Storing and Shuttling Electrons with Reduced Graphene Oxide, *Nano Lett*., 2010, **10**, 577–583.

Photochemical & Photobiological Sciences Accepted Manuscript

9. A. Pandikumar and R. Ramaraj, Titanium dioxide–gold nanocomposite materials embedded in silicate sol–gel film catalyst for simultaneous photodegradation of hexavalent chromium and methylene blue, *J. Hazard. Mater*., 2012, **203–204**, 244–250.
10. A. Pandikumar, S. Murugesan and R. Ramaraj, Functionalized Silicate Sol−Gel-Supported TiO_2−Au Core−Shell Nanomaterials and Their Photoelectrocatalytic Activity, *ACS Appl. Mater. Interfaces*, 2010, **2**, 1912–1917.
11. X. Zhao, M. Yin, L. Ma, L. Liang, C. Liu, J. Liao, T. Lu and W. Xing, Recent advances in catalysts for direct methanol fuel cells, *Energy Environ. Sci*., 2011, **4**, 2736–2753.
12. J. Mitzel, F. Arena, T. Walter, S. Stefener and R. Hempelmann, Direct Methanol Fuel Cell – Alternative Materials and Catalyst Preparation, *Z. Phys. Chem*., 2013, **227**, 497–540.
13. M. Hepel, I. Kumarihamy and C. J. Zhong, Nanoporous TiO_2-supported bimetallic catalysts for methanol oxidation in acidic media, *Electrochem. Commun*., 2006, **8**, 1439–1444.
14. K. Drew, G. Girishkumar, K. Vinodgopal and P. V. Kamat, Boosting Fuel Cell Performance with a Semiconductor Photocatalyst: TiO_2/Pt−Ru Hybrid Catalyst for Methanol Oxidation, *J. Phys Chem. B*, 2005, **109**, 11851–11857.
15. J. Pradhan, S. N. Das and R. S. Thakur, Adsorption of Hexavalent Chromium from Aqueous Solution by Using Activated Red Mud, *J. Colloid Interf. Sci*., 1999, **217**, 137–141.
16. C. R. Chenthamarakshan, K. Rajeshwar and E. J. Wolfrum, Heterogeneous Photocatalytic Reduction of Cr(VI) in UV-Irradiated Titania Suspensions: Effect of Protons, Ammonium Ions, and Other Interfacial Aspects, *Langmuir*, 2000, **16**, 2715–2721.
17. S. D. Perera, R. G. Mariano, K. Vu, N. Nour, O. Seitz, Y. Chabal and K. J. Balkus, Hydrothermal Synthesis of Graphene-TiO_2 Nanotube Composites with Enhanced Photocatalytic Activity, *ACS Catal*., 2012, **2**, 949–956.
18. N. M. Stover, Diphenylcarbazide as a test for Chromium, *J. Am. Chem. Soc*., 1928, **50**, 2363–2366.
19. A. Ambrosi, C. K. Chua, A. Bonanni and M. Pumera, Lithium Aluminum Hydride as Reducing Agent for Chemically Reduced Graphene Oxides, *Chem. Mater*., 2012, **24**, 2292–2298.

Photochemical & Photobiological Sciences Accepted Manuscript

20. V. Subramanian, E. Wolf and P. V. Kamat, Semiconductor-Metal Composite Nanostructures. To What Extent Do Metal Nanoparticles Improve the Photocatalytic Activity of TiO_2 Films?, *J. Phys. Chem. B* **2001**, 105, 11439-11446.

21. G. Williams and P. V. Kamat, Graphene−Semiconductor Nanocomposites: Excited-State Interactions between ZnO Nanoparticles and Graphene Oxide, *Langmuir,* 2009, **25**, 13869–13873.

22. A. Dawson and P. V. Kamat, Semiconductor−Metal Nanocomposites. Photoinduced Fusion and Photocatalysis of Gold-Capped TiO_2 (TiO_2/Gold) Nanoparticles, *J. Phys. Chem. B,* 2001, **105**, 960–966.

23. L-W. Zhang, H-B. Fu and Y-F. Zhu, Efficient TiO_2 Photocatalysts from Surface Hybridization of TiO_2 Particles with Graphite-like Carbon, *Adv. Funct. Mater.,* **2008**, 18, 2180–2189.

Photochemical & Photobiological Sciences Accepted Manuscript

Graphical abstract

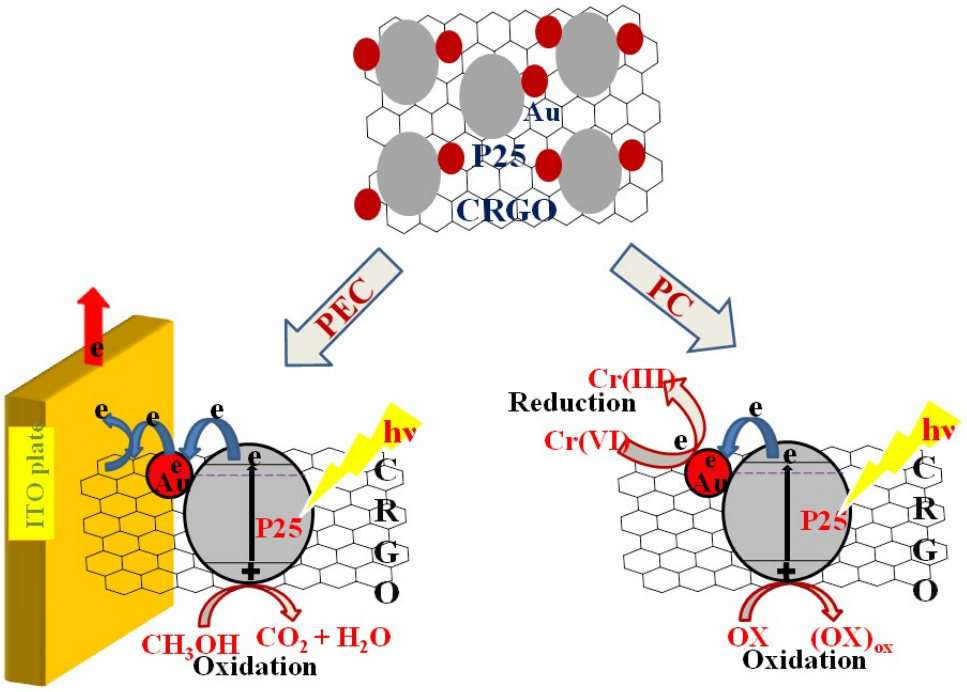

PEC = Photoelectrochemical
PC = Photocatalytic

Research highlights

- ✓ CRGO–P25–Au NCMs were prepared through a one-pot chemical reduction method.
- ✓ Photoelectrocatalytic oxidation of methanol by CRGO–P25–Au(1) modified photoelectrode exhibited higher photocurrent.
- ✓ Efficient photocatalytic reduction of toxic Cr(VI) ions to Cr(III) ions observed at the CRGO–P25–Au(3) NCM.

Photochemical & Photobiological Sciences Accepted Manuscript